In Situ Visualization of Birth and Annihilation of Grain Boundaries in an Au Nanocrystal

He Zheng, Jianbo Wang, Jian Yu Huang, Ajing Cao, and Scott X. Mao

Phys. Rev. Lett. **109**, 225501 — Published 28 November 2012

DOI: 10.1103/PhysRevLett.109.225501

In-situ visualization of "birth" and annihilation of grain boundary in Au nano-crystal

He Zheng,[1,2] Jianbo Wang,[1*] Jian Yu Huang,[3*] Ajing Cao,[4] Scott X. Mao[2*]

[1]School of Physics and Technology, Center for Electron Microscopy and MOE Key Laboratory of Artificial Micro- and Nano-structures, Wuhan University, Wuhan 430072, China

[2]Department of Mechanical Engineering & Materials Science, University of Pittsburgh, Pittsburgh, Pennsylvania 15261, USA

[3]Center for Integrated Nanotechnologies, Sandia National Laboratories, Albuquerque, New Mexico 87185, USA

[4]MST-8, Los Alamos National Laboratory, Los Alamos, New Mexico 87544, USA

*e-mail: wang@whu.edu.cn; jyhuang8@yahoo.com; smao@engr.pitt.edu

Abstract

The formation and vanishing processes of a low angle grain boudary (GB) in nanosized Au during tension and release of stress, respectively, were obsvered by *in-situ* high resolution transmission electron microscopy. The nucleation of perfect dislocations led to the formation of a 15^{o} low angle GB inside an Au nanocrystal upon off-axial tensile loading (coupled uniaxial tensile and bending stress). Strikingly, the dislocations were completely annihilated accompanied with the disappearance of GB after the removal of external stress, indicating that the plastic bending is recoverable in the nano-crystal. The back force and surface stress played important roles in such a pseudo-elastic behavior. This transient GB dynamics cannot be captured in *ex-situ* experimental investigations. Such pseudo-elastic bending deformation in nanosized crystal will have important impact on the designing of nano-mechanical device with ultra-high bending capability.

Fundamental understandings of the mechanical properties of nano-scale materials are crucial for realizing their potential applications in the next generation nano-devices. Owing to high surface-to-volume ratio, nano-scale materials including nanowires (NWs) [1], nanopillars [2] and nanobeams [3], behave differently compared to their bulk counterparts. For instance, several novel structures have been proposed for wires with a few nanometers in diameter such as helical multi-shell gold NWs [1], and "non-crystalline" structures of aluminum and lead NWs [4].

Interestingly, different mechanical behaviors of face-centered cubic (FCC) nano-crystals have been revealed under various stress conditions. To be specific, under external tensile or compressive stress, the plasticity was shown to be dominated by the surface-mediated discrete partial dislocation activity as predicted by both molecular dynamics (MD) simulations [5-7] and verified by recent experimental observations [8]. Meanwhile, it was observed that the partial dislocations could easily escape to the free surface. Thus, the plastic deformation of nano-sized materials (e.g. NWs and nanopillars) exhibited limited or no strain hardening at all, as exemplified by the sharp stress drop after the initial yielding point in the stress-strain curves predicted from MD simulations. In stark contrast, a significant strain hardening has been unveiled in Au NWs, by utilizing an in-contact atomic force microscope (AFM) to apply bending moment on an individual NW in a single or double clamped configuration [9,10]. It was suggested that the interactions between dislocations and grain boundaries, similar to the hardening mechanisms in bulk materials, may still operate at the nano-scale. Nonetheless, since AFM falls short in probing the

atomic-scale structural information, the intuitive perspective concerning the deformation process still remains obscure.

In the present study, with the advent of recently developed *in-situ* high resolution transmission electron microscopy (HRTEM) technique [8], off-axial tensile loading (coupled uniaxial tensile and bending stress) of single crystalline gold crystal with size around 10 nm (Fig. 1) was carried out inside an FEI Tecnai F30 field emission gun transmission electron microscope operated at 300 kV, aided by Nanofactory TEM – scanning tunneling microscopy (STM) platform. Detailed sample preparation and experimental method can be found in our previous work [8]. Here, we show that, the full dislocations could be formed by the coalescence of leading and trailing partial dislocations nucleated from the free surface. Due to the bending stress, the dislocations piled up and formed a low angle grain boundary (GB) inside the nano-crystal, which may contribute to the strain-hardening as observed previously [9]. Strikingly, upon the release of external stress, the dislocations were completely annihilated accompanied with the disappearance of GB, representative of a pseudo-elastic behavior in nano-scale FCC single crystal. Although such behavior has been investigated extensively by theoretical modeling [11-13], no direct experimental evidence has been revealed hitherto.

The tapered single crystal gold shown in Fig. 1(a) is under off-axial tensile loading, the direction of which is designated by letter "σ", forming an angle of 15^{o} with the axial direction [002]. The displacement rate is 4.9×10^{-2} nm/s. The viewing direction is along $[1\bar{1}0]$ zone axis, which allows us to directly observe the dislocation

activities in FCC crystal. Evidently, in the image plane, the crystal was subjected to a bending force along the $[110]$ direction (Fig. 1(a)) besides the uniaxial tensile loading along the $[002]$ direction. In current case, it is believed that the out-of-plane stress along $[1\bar{1}0]$ direction is negligible and will not exert considerable effect on the deformation behavior. As expected, the crystal elongated while its diameter decreased under the tensile stress (Figs. 1(b)-1(d)), induced by the surface-mediated partial dislocation activity as will be discussed in Fig. 2. Meanwhile, under bending stress, the axial direction of the right side crystal with smaller diameter was gradually altered (Figs. 1(b)-1(d)) while that of the left side crystal remained fixed (indicated by the arrows in Figs. 1(a) and 1(d)). Further HRTEM analysis was carried out to reveal the associated dynamic process.

Surface mediated partial dislocation activity was found to be the major plastic deformation mechanism, in full agreement with our previous study [8]. The nucleation and propagation of a leading partial dislocation, with a stacking fault (SF) left behind, is presented in Fig. 2(a). In addition, deformation twinning, which occurrs when nucleation of a leading partial dislocation is followed by a twinning partial dislocation on the adjacent $\{111\}$ slip plane, was also observed (indicated by double arrow heads in Fig. 2(b)). The simulated HRTEM images [14] indicate that the dark spots in Figs. 2(a)-2(b) represent the Au atom columns. Figure 2(c) displays a Fourier filtered image of a boxed area in Fig. 2(a), showing the alteration from FCC to hexagonal close-packed (HCP) stacking sequence (see also Fig. S2 in [14]) by introducing a SF (pointed out by arrow head). Such dislocation dynamics led to the elongation of the crystal.

Simultaneously, the bending stress altered the orientation of the right thinner part of the crystal. Afterwards, the propagation of the leading partials were blocked at some certain point inside the crystal as a result of local stress concentration (pointed out by arrow head in Fig. 2(b)), which is primarily due to the increasing Peierls–Nabarro stress (lattice resistance to dislocation motion) on the curved slip planes under bending deformation [15,16]. Similar phenomenon is shown in Figs. 1(b) and 1(c) as well. During further deformation, the trailing partial dislocation nucleated from the same (111) slip plane interacted with the foregoing leading partial to form a full dislocation. The whole process can be schematically illustrated by drawing one facet (i.e. (111) plane) of the Thompson tetrahedron in Fig. 2(d). For instance, a full dislocation with Burgers vector of $\vec{C}\vec{B}$ can be obtained via the following reaction:

$$\vec{C}\vec{\delta} + \vec{\delta}\vec{B} \rightarrow \vec{C}\vec{B} \qquad (1)$$

whereas $\vec{C}\vec{\delta}$ and $\vec{\delta}\vec{B}$ are the Burgers vectors of the leading and trailing partial dislocation, respectively.

Accompanied with further plastic deformation, more and more full dislocations nucleated. The average distance between them decreased and dislocations started to block the motion of each other. In this manner, strain hardening is expected as a result of the formation of dense network of dislocation jogs [17] which requires larger stress to sustain the subsequent plasticity. Thereby, we present a direct experimental evidence showing that strain hardening can be realized in the single FCC nano-crystal under complicated stress loading conditions, consistent with previous report [9]. Before the fracture of the nano-crystal, a low angle GB (Fig. 3(a)) was eventually

generated by the lattice distortion induced by the full dislocation pile-ups. The mis-orientation angle across the GB is measured to be ~15^{o}. Furthermore, the axial direction of reoriented crystal is parallel with the initial loading direction "σ". It is worthy of noting that the diffraction contrast in the vicinity of the grain boundary may be affected by the Moire fringe, which results from the inclination of the grain boundary to the observation direction, and (or) delocalization effect, which is a typical effect regarding the transmission electron microscope without the spherical aberration corrector [18]. The Fourier-filtered image (Fig. 3(b)) of the boxed area in Fig. 3(a) suggests that there are two types of dislocations with different Burgers vectors of $1/2[101]$ or $1/2[011]$ (designated by the black "T", hereafter referred as type I dislocations) and $1/2[\bar{1}01]$ or $1/2[0\bar{1}1]$ (designated by the red "T", hereafter referred as type II dislocations), which have an angle of 60^{o} or 120^{o} with respect to the dislocation line (see also Fig. S3 in [14]). The GB plane was curved from (002) to (111) plane (sketched by the dashed lines in Fig. 3(a)), spanning from the upper to lower bound of the GB. Meanwhile, both types of dislocations along the (002) GB were periodically spaced. The averaged inter-spacings of type I and II dislocations are 1.6 nm and 1.4 nm, respectively.

Surprisingly, when the external stress was released, the initially nucleated GB suddenly vanished; and the full dislocations disappeared as illustrated in Fig. 3(c). The axial direction of the right nano-crystal reoriented back to the initial orientation (Fig. 1(a)) spontaneously, indicating that the bending strain was fully recovered. Serving as an eyeguide, black arrowheads in Fig. 3(c) point out the two ends of the initially formed GB. Such reversible bending strain has never been discovered in the

bending tests of samples with micrometer size [19]. The entire recoverable process occurred in quite a short time period, i.e. within 0.5 s (the limit of our acquisition time). The deformation process described herein is provided in movie M1, available as supplemental material in [14].

Although the corresponding dislocation activity was not recorded due to the limit of the capture rate (2 frames per second), the underlying physical mechanism can be well understood for that the dislocations can be drawn back to the surface area by the image force [20] and the back force at the moment fracture occurs. Here, we stress that the recoverable plasticity can only occur in nano-scale materials, due to the large image forces of dislocation with the presence of free surfaces, which serves as the driving force for dislocation annihilation at the free surfaces. Recent theoretical work regarding the bending of micrometer-sized beams revealed that, owing to the image force, the surface regions are relatively denuded of dislocations as compared with the central part [21]. Theoretically, image force exerted on dislocations per unit length can be calculated as:

$$\frac{F}{L} = \frac{\mu b^2}{4\pi(1-\upsilon)l} \tag{2}$$

Where F, l, μ, b being the force, the distance to free surface, the shear modulus, and the magnitude of Burgers vector, respectively [22]. Clearly, the line force F/L acting on dislocation is inversely proportional to l, which can be deemed as the nano-scale crystal width in this case. The smaller sample dimensions, the bigger force drives the dislocation out of the system. It has been theorized that for the crystals below a critical size (e.g. 36 nm for Al), the image force experienced by the dislocation can exceed the Peierls–Nabarro force [23]. This will leads to dislocation leaving the

crystal without the application of an external stress and thus making it dislocation free. The Peierls–Nabarro stress of FCC crystals is calculated to be on the order of $1.5\times 10^{-3}\mu$ [24-26], based upon which the Peierls–Nabarro stress in Au is estimated to be 40.5 MPa. This stress level required for dislocation movement is relatively small such that the chance for the dislocation to escape the nano-scale crystal increases due to the image force. We are aware that recent experimental observation has revealed the recoverable plastic deformation (i.e. pseudo-elasticity) in free-standing nanocrystalline aluminum and gold thin films [27]. The recovery process is thermally activated. Furthermore, previous works have shown the morphology change in Au nanoparticles accompanied with the increasing temperature (up to 1000 K) [28,29]. In the current experiment, the temperature rise in Au crystal is negligible due to the high thermal conductivity of Au (300 W/(mK)) and low electron beam current density (80 A cm^{-2}) applied to get the HRTEM images. Moreover, as discussed by Williams [30], it is unlikely that the radiation will be a significant factor unless the thermal contact is very poor. For that the gold nano-crystal was well-attached to a gold thin film in our experiment which could dissipate the accumulated heat in the nano-crystal quickly, it is convincible that the beam heating effect is not significant. Thus, the thermal gradient will not play a major role for the recoverable plastic strain we observed.

In summary, we have conducted *in-situ* high resolution transmission electron microscopy observations of Au crystal with size of several nanometers undergoing off-axial strain. Real-time video indicates the formation of a 15^{o} low angle GB due to the full dislocation pile-ups. Strikingly, the dislocations were completely annihilated accompanied with the disappearance of GB after the removal of the external stress.

The imaging force played important roles in such a pseudo-elastic behavior. These results constitute the experimental evidence of recoverable plasticity in nanoscale materials, and serve as guidance to the design of nano-devices with ultra-high bending capability for advanced applications. Given that both the GB formation mechanism and annihilation of dislocations at free surfaces are not specific to particular metals, the conclusion should be generally applicable to other nano-sized FCC crystals.

Acknowledgements

This work was supported by 973 Program (2011CB933300), National Natural Science Foundation of China (51071110, 40972044, 51271134, J1210061), China MOE NCET Program (NCET-07-0640), MOE Doctoral Fund (20090141110059), and the Fundamental Research Funds for the Central Universities. S.M. acknowledges NSF CMMI 08 010934 through University of Pittsburgh and Sandia National Lab support. This work was performed, in part, at the Center for Integrated Nanotechnologies, a U.S. Department of Energy, Office of Basic Energy Sciences user facility. Sandia National Laboratories is a multi-program laboratory managed and operated by Sandia Corporation, a wholly owned subsidiary of Lockheed Martin Corporation, for the U.S. Department of Energy's National Nuclear Security Administration under contract DE-AC04-94AL85000. H.Z. would like to thank the Chinese Scholarship Council for financial support. The authors thank Hongqian Sang and Shuangfeng Jia from Wuhan University for their kindness help in the HRTEM simulation.

References

[1] Y. Kondo and K. Takayanagi, *Science* **289**, 606 (2000).

[2] A. T. Jennings, M. J. Burek, and J. R. Greer, *Phys. Rev. Lett.* **104**, 135503 (2010).

[3] S. Zhang, I. S. Kim, and L. J. Lauhon, *Nano Lett.* **11**, 1443 (2011).

[4] O. Gülseren, F. Ercolessi, and E. Tosatti, *Phys. Rev. Lett.* **80**, 3775 (1998).

[5] K. Gall, J. Diao, and M. L. Dunn, *Nano Lett.* **4**, 2431 (2004).

[6] E. Rabkin and D. J. Srolovitz, *Nano Lett.* **7**, 101 (2006).

[7] T. Zhu, J. Li, A. Samanta, A. Leach, and K. Gall, *Phys. Rev. Lett.* **100**, 025502 (2008).

[8] H. Zheng *et al.*, *Nat. Commun.* **1**, 144 (2010).

[9] B. Wu, A. Heidelberg, and J. J. Boland, *Nature Mater.* **4**, 525 (2005).

[10] B. Wu *et al.*, *Nano Lett.* **6**, 468 (2006).

[11] J. Diao, K. Gall, and M. L. Dunn, *Phys. Rev. B* **70**, 075413 (2004).

[12] D. Mordehai, E. Rabkin, and D. J. Srolovitz, *Phys. Rev. Lett.* **107**, 096101 (2011).

[13] H. S. Park, K. Gall, and J. A. Zimmerman, *Phys. Rev. Lett.* **95**, 255504 (2005).

[14] See supplemental material for HRTEM simulation results and movie M1.

[15] B. Joós and M. S. Duesbery, *Phys. Rev. Lett.* **78**, 266 (1997).

[16] F. R. N. Nabarro, *Mater. Sci. Eng., A* **234–236**, 67 (1997).

[17] X. Tian, J. Cui, and M. Xiang, *J. Comput. Theor. Nanosci.* **7**, 1194 (2010).

[18] S. Bals, B. Kabius, M. Haider, V. Radmilovic, and C. Kisielowski, *Solid State Commun.* **130**, 675 (2004).

[19] C. Motz, D. Weygand, J. Senger, and P. Gumbsch, *Acta Mater.* **56**, 1942 (2008).

[20] B. Q. Li, M. L. Sui, B. Li, E. Ma, and S. X. Mao, *Phys. Rev. Lett.* **102**, 205504 (2009).

[21] C. Motz and D. J. Dunstan, *Acta Mater.* **60**, 1603 (2012).

[22] J. P. Hirth and J. Lothe, *Theory of Dislocations* (John Wiley and Sons, New York, 1992).

[23] P. Khanikar and A. Subramaniam, *J. Nano Res.* **10**, 93 (2010).

[24] M. Bujard, G. Gremaud, and W. Benoit, *J. Appl. Phys.* **62**, 3173 (1987).

[25] L. Wang, Z. Zhang, E. Ma, and X. D. Han, *Appl. Phys. Lett.* **98**, 051905 (2011).

[26] G. Lu, N. Kioussis, V. V. Bulatov, and E. Kaxiras, *Phys. Rev. B* **62**, 3099 (2000).

[27] J. Rajagopalan, J. H. Han, and M. T. A. Saif, *Science* **315**, 1831 (2007).

[28] M. A. van Huis *et al.*, *Adv. Mater.* **21**, 4992 (2009).

[29] Y. K. Mishra, S. Mohapatra, D. K. Avasthi, N. P. Lalla, and A. Gupta, *Adv. Mat. Lett.* **1**, 151 (2010).

[30] P. Williams, *Appl. Phys. Lett.* **50**, 1760 (1987).

Figure Captions

FIG. 1. Sequential TEM images of the tapered single nano-crystal Au under off-axial tensile stress. The arrows in (a) and (d) show the axial direction of the crystal.

FIG. 2 (color online). HRTEM images showing the occurrence of stacking fault (a) and twinning (b) induced by the surface nucleated partial dislocations. The annotations "M" and "T" stand for matrix and twin, respectively. (c) Fourier filtered image of the boxed area in (a) showing the alteration from FCC to HCP stacking ordering when a stacking fault is present. (d) Schematic drawing of slip directions inside a (111) plane. The black and red lines represent the Burgers vectors of full and partial dislocations, respectively.

FIG. 3 (color online). (a) A low angle GB formed due to the full dislocation pile-ups. (b) Fourier filtered image of the enclosed area in (a) showing the detailed GB configuration. (c) The disappearance of the GB accompanied with the release of external stress. The white lines are guidance for eyes, showing the relative mis-orientation angle between the crystals across the GB. Arrow points out the location where fracture occurs.

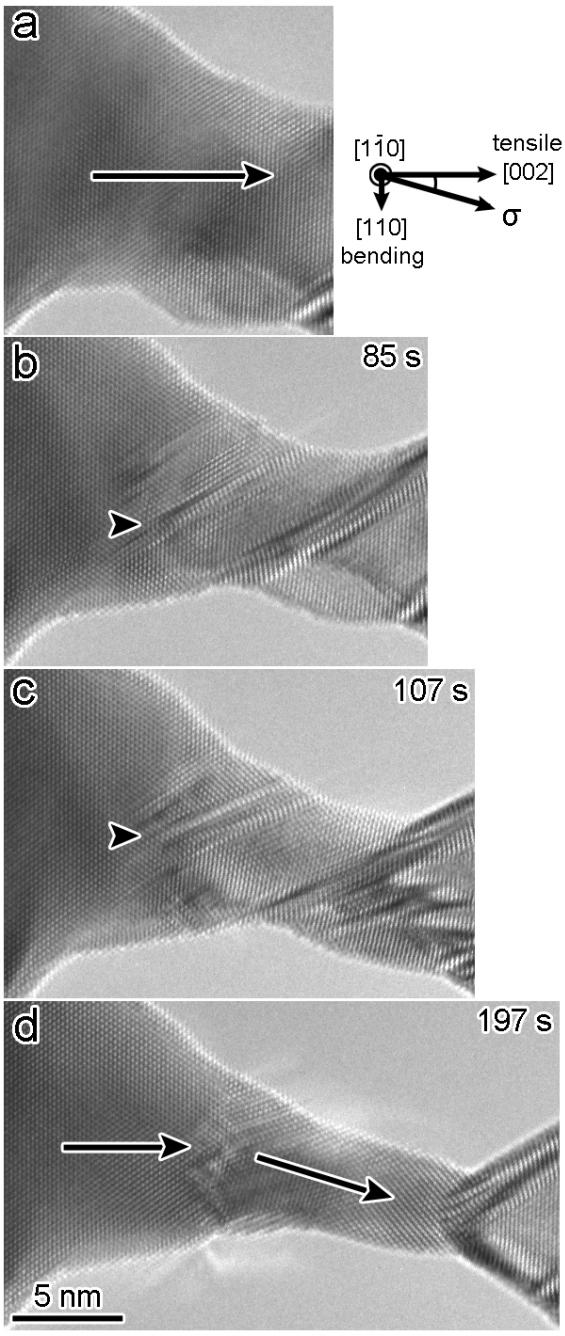

Figure 1

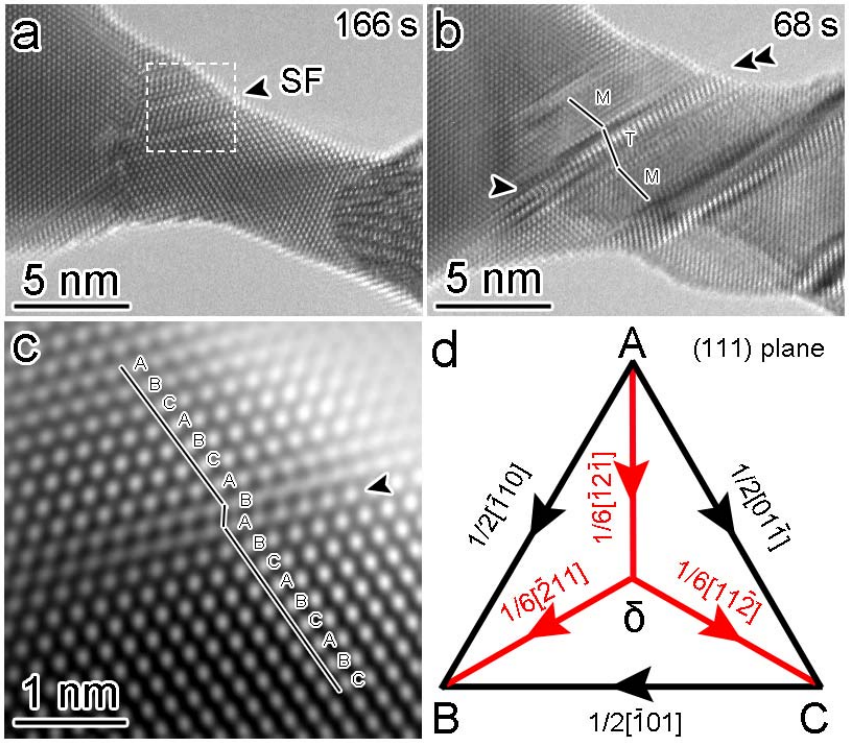
a
166 s
SF
5 nm
b
68 s
M
T
M
5 nm
c
A
B
C
A
B
C
A
B
A
B
C
A
B
C
A
B
C
1 nm
d
A
(111) plane
1/2[1̄10]
1/6[1̄2̄1]
1/2[01̄1̄]
1/6[2̄11]
δ
1/6[11̄2̄]
B
1/2[1̄01]
C

Figure 2

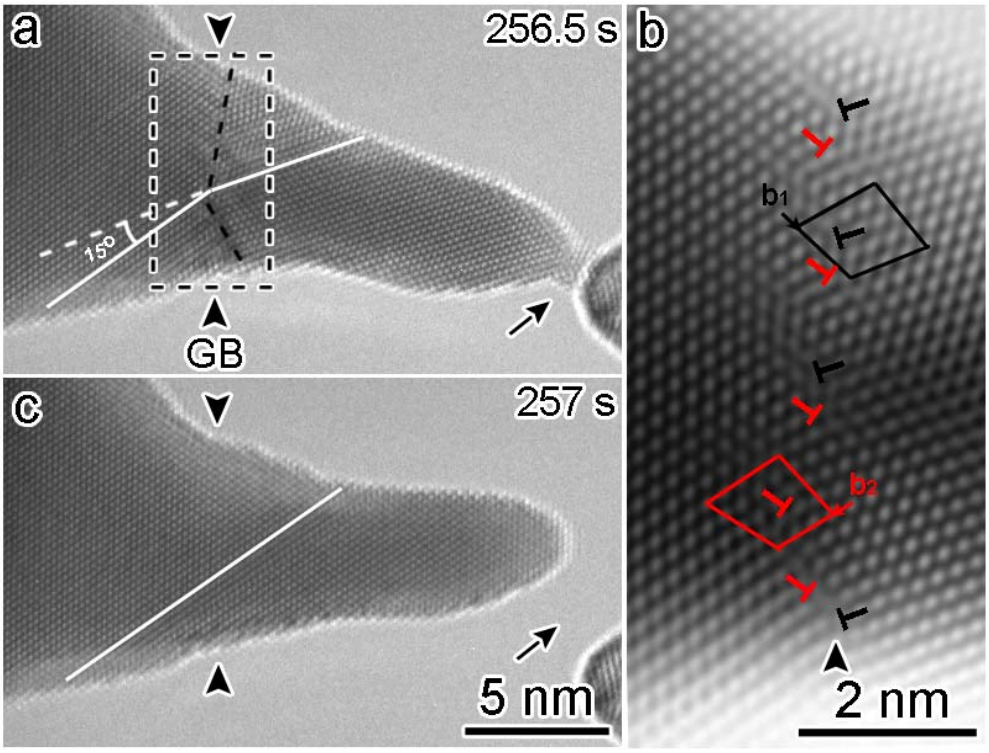

Figure 3